 CMES, vol.93, no.6, pp.441-468, 2013

Modeling of Moisture Diffusion in Permeable Particle-Reinforced Epoxy Resins Using Three-Dimensional Heterogeneous Hybrid Moisture Element Method

D.S. Liu[1,2], Z.H. Fong[1], I.H. Lin[1], Z.W. Zhuang[1]

Abstract: In this study, we proposed a novel numerical technique to simulate the transient moisture diffusion process and to apply it to heterogeneous composite resins. The method is based on a heterogeneous hybrid moisture element (HHME), with properties determined through an equivalent hybrid moisture capacitance/conductance matrix that was calculated using the conventional finite element formulation in space discretization and the θ-method in time discretization, with similar mass/stiffness properties and matrix condensing operations. A coupled HHME with finite element scheme was developed and implemented in the computer code by using the commercial software MATLAB to analyze the transient moisture diffusion process of composite materials that contain multiple distributed particles and possess permeable capability.

The HHMEM proposed in this study provides a straightforward and efficient means of modeling because only one HHME moisture characteristic matrix needs to be calculated for all HHMEs that share the same characteristics. Crucial sealing adhesive particle parameters, such as the size, moisture diffusion coefficient, and volume fraction of particles in the composite resin, can be easily investigated by controlling the size of the inclusion region within the HHME domain. Several numerical examples demonstrate the effectiveness and accuracy of the present methodology.

Keywords: 3D-HHMEM, Theta method, Permeable particles, Transient moisture diffusion.

[1] Advanced Institute of Manufacturing for High-tech Innovations and Department of Mechanical Engineering, National Chung Cheng University, 168, University Rd., Min-Hsiung, Chia-Yi, 621, Taiwan, R.O.C.

[2] Corresponding author. Tel.: +886-5-2720411 (Ext: 33305); fax: +886-5-2720589; Email: imedsl@ccu.edu.tw (D.S. Liu).

1 Introduction

Moisture ingress through the sealing zone of electronic products has a major effect on the degradation and life the product. Preventing moisture permeation through the sealing zone is a key design concern. One way to improve the moisture-delay capabilities of the sealing materials is to add permeable particles to the sealing adhesive. Polymer composites absorb moisture during their service life, principally through the resin matrix and through the fibers, when they are permeable [Tsai and Hahn (1980)]. The moisture affects the mechanical properties of composites, binding capacities, and interfaces within the product. Because of these effects, determining how quickly moisture diffuses into the composite is an interesting study.

The moisture-diffusion characteristics of composites have attracted considerable attention [Shen and Springer (1977); Browning, Husman, and Whitney (1977)]. Typically, transient moisture diffusion in normal environmental conditions is similar to a Fickian process. Thus, the analytical models designed to explore the moisture diffusion characteristics are drawn from a homogenized model. In homogeneous materials, the transport of moisture is governed by (1) the maximum moisture content, and (2) the effective diffusivity, which typically varies as a function of temperature and the volume fraction of the particles. However, the effective or average properties ignore the micro-structural heterogeneity. Thus, the homogenized rule-of-mixtures approach may not effectively describe the time-dependent moisture content field in transient conditions [Vaddadi, Nakamura, and Singh (2003a,b)].

Researchers have expended great efforts to develop various numerical techniques for modeling and calculating heterogeneous materials that contain imbedded inclusions and a surrounding inter-phase. A numerical model, called the representative volume element (RVE), was proposed to represent particle-reinforced composites [Yang, Yang, Ma and Liu (2010); Stoeven, Askes and Sluys (2004)]. Several studies have analyzed the RVE model to determine the effective moisture diffusivity of composite material. The RVE was chosen as the basic cell of the composite medium. However, some issues need to be carefully addressed when conducting such analyses. First, the RVE that correctly corresponds to the assumed particle distribution must be isolated. Second, the correct boundary conditions must be applied to the chosen RVE to model the various load situations.

The conventional finite element method (FEM) is commonly employed in such situations because it provides a convenient way to understand the mechanical behavior of particle-reinforced composites [e.g., Kawaguchi and Pearson (2003); Vaddadi, Nakamura and Singh (2003b); Pahr and Böhm (2008); Takashima, Nakagaki and Miyazaki (2007)]. However, a large number of fine finite elements are required and mesh modeling is generally a tedious and complicated task, particularly when

the aim is to clarify the relationship between the volume fraction of the fibers and the specific property of the materials. The T-Trefftz Voronoi Cells finite elements (VCFEM-TTs) are developed to solve composite and porous materials with orders of less computational burden. [Dong, L. and Atluri, S. N. (2012a)] discussed developments in VCFEM-TTs with elastic/rigid inclusions or voids. [Dong, L.and Atluri, S. N. (2012b,c)] extended the VCFEM-TTs to solve 3D problems with spherical and ellipsoidal inclusions or voids.

In a series of related studies, [Liu and Chiou (2003a, b, 2005)] discussed developments in 2-D and 3-D infinite element methods (IEM). The conventional IEM approach was implemented through computer code to manage the various types of classic elasticity and singularity problems. [Liu, Chiou and Chen (2004, 2005)] extended the IEM to address elastostatic problems in which the constituent material properties were heterogeneous. [Liu, Zhuang and Chung (2009, 2011)] also extended the IEM to address moisture diffusion problems, in which the constituent material properties were heterogeneous. These earlier works are summarized in the literature [Guo (1979); Ying (1995)]. However, until now, IEM moisture diffusion analysis has been limited to the solution of 2-D problems. Developed in this study is a novel, efficient, and convenient numerical technique, known as the 3-D heterogeneous hybrid moisture element method (3D-HHMEM), to characterize transient moisture diffusion in composite materials that possess permeable particles. The proposed numerical method is used to study the transient moisture diffusion process. This includes the effects brought about by variations in the volume fraction on the rate of moisture diffusion. Furthermore, a crucial material property, known as the effective diffusion coefficient, can be found by an iterative calculation method. This parameter can be applied to simulate moisture diffusion problems and reduce the calculation time in numerical analysis.

2 The 3-D heterogeneous hybrid moisture element method

In this section, an HHME formulation is derived for modeling the 3-D transient moisture diffusion problem. The basis of the proposed method is an HHME possessing an elastic inclusion or a void of arbitrary geometry (e.g., a circle), as shown in Fig. 1(a). The element domain is decomposed into two separate sub-domains, as shown in Fig. 1(b) and (c), each with dissimilar material characteristics. The two domains represent, respectively, (1) the inter-phase sub-domain that possess boundaries Γ_0 and Γ_s, and (2) the inclusion sub-domain with a boundary Γ_s. Γ_0 and Γ_s comprise, respectively, in which the element's outer boundary is accompanied by neighboring elements and the inner interface between the interphase and the inclusion sub-domains.

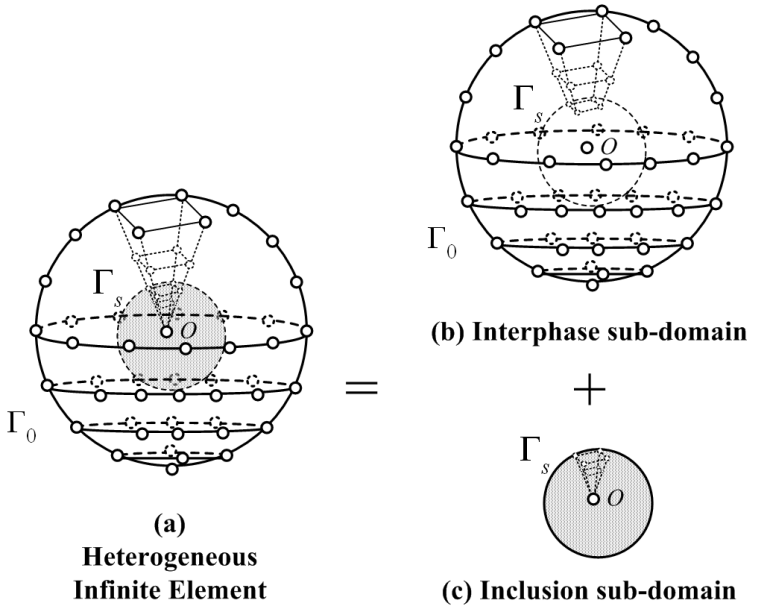

Figure 1: Element decomposition: (a) heterogeneous hybrid moisture element; (b) inter-phase sub-domain; and (c) inclusion sub-domain

2.1 Governing equation of moisture diffusion

In the existing modeling method, the transient moisture diffusion equation is analogous to that of heat conduction. The analogous technique for a homogeneous material system [Crank and Park (1956)] has recently been extended to include a multi-material system [Wong, Teo and Lim (1998); Wong, Rajoo, Koh and Lim (2002)], and hence it is suitable for the analysis of moisture diffusion in a heterogeneous composite material filled with permeable fibers.

To enforce continuity across a bi-material interface for modeling of moisture diffusion in a multi-material system, a moisture wetness variable, W, is introduced. W is defined as

$$\mathrm{W} = \frac{C}{C_{\mathrm{sat}}}, \quad 1 \geq \mathrm{W} \geq 0. \tag{1}$$

where C and C_{sat} are, respectively, the moisture concentration and the maximum moisture concentration that can be absorbed by the material. The lower limit of W, i.e. $\mathrm{W} = 0$, indicates that the material is completely dry, while the upper limit, i.e. $\mathrm{W} = 1$, indicates that the material is fully saturated with moisture. The "wetness" thermal-moisture analogy scheme for the current finite element implementation is

presented in Tab. 1.

Table 1: FEA thermal-moisture analogy for moisture diffusion modeling

Properties	Thermal	Moisture
Field variable	Temperature, T	Wetness, W
Density	ρ (kg/m^3)	1
Conductivity	K (W/m $\cdot^\circ C$)	$D * C_{\text{sat}}$ (kg/s $\cdot$ m)
Specific capacity	c (J/kg $\cdot^\circ C$)	C_{sat} (kg/m^3)

Consider a 3-D ball region with a boundary s. The differential equation for the 3-D moisture diffusion problem is given by

$$\frac{\partial W}{\partial x}\left(D_x\frac{\partial W}{\partial x}\right)+\frac{\partial W}{\partial y}\left(D_y\frac{\partial W}{\partial y}\right)+\frac{\partial W}{\partial z}\left(D_z\frac{\partial W}{\partial z}\right)=\frac{\partial W}{\partial t}. \tag{2}$$

and has boundary conditions of

$$W=W_0\,|_{s=s_D} \quad \text{and} \quad D_x n_x\frac{\partial W}{\partial x}+D_y n_y\frac{\partial W}{\partial y}+D_z n_z\frac{\partial W}{\partial z}=f_B\,|_{s=s_N}\,. \tag{3}$$

where D_x, D_y and D_z are the moisture diffusion coefficients for the x-, y- and z-directions, respectively, n_x, n_y and n_z are directional cosines, and f_B is the boundary flux, which has a positive value when directed into the body of interest. Let s_D and s_N respectively denote the parts of s where the Dirichlet and Neumann boundary conditions are specified, where $s=s_D\cup s_N$ and $s_D\cap s_N=\emptyset$.

The unit element matrix equation can be obtained from the governing differential equation, Eq. (2), by applying Galerkin's weighted residual approach. The resulting element matrix equation has the form

$$[M_e]\{\dot{W}_e\}+[K_e]\{W_e\}=\{P_e\}, \tag{4}$$

in which the element moisture capacitance matrix is given by

$$[M_e]=\int [N]^T[N]\,dxdydz, \tag{5}$$

the element moisture conductance matrix has the form

$$[K_e]=\int [B]^T[D][B]\,dxdydz, \tag{6}$$

and finally

$$\{P_e\} = \int [N]^T f_B \, ds_N. \tag{7}$$

Note that in the equations above, $[B]$ and $[N]$ denote the shape function derivative matrix and the shape function matrix, respectively.

The diffusivity matrix is given by

$$[D] = \begin{bmatrix} D_x & 0 & 0 \\ 0 & D_y & 0 \\ 0 & 0 & D_z \end{bmatrix}. \tag{8}$$

For the time discretization of the system of ordinary differential equation, Eq. (4), we apply the well-know θ-method [Lewis, Morgan, Thomas and Seetharamu (1996)], which results in the equation

$$(M_e + \theta \cdot \Delta t \cdot K_e) \cdot W_e^{n+1} = [M_e - (1-\theta) \cdot \Delta t \cdot K_e] \cdot W_e^n + \Delta t \cdot P_e. \tag{9}$$

Let $\phi = \theta - 1$ and substitute it into Eq. (9), get

$$(M_e + \theta \cdot \Delta t \cdot K_e) \cdot W_e^{n+1} = [M_e + \phi \cdot \Delta t \cdot K_e] \cdot W_e^n + \Delta t \cdot P_e, \tag{10}$$

where W_e^n denotes the known moisture wetness at the current time t_n, the time increment Δt is defined as $\Delta t = t_{n+1} - t_n$ and $(M_e + \theta \cdot \Delta t \cdot K_e)$ denotes the combined moisture capacitance/conductance matrix. Clearly, this is a system of linear algebraic equations with respect to the unknown vector W_e^{n+1} as the approximation of the moisture wetness at the new time-level t_{n+1}. Here the parameter θ is related to the applied numerical method and is an arbitrary parameter on the interval [0, 1]. It is worth emphasizing that in $\theta = 0.5$, the method yields the Crank-Nicolson implicit method which produces a higher accuracy for time discretization [Crank and Nicolson (1947)]. Therefore, the parameter θ in the current numerical analysis is set as 0.5.

Another practical consideration was a proper time increment. If the time increment is not selected properly, the results can exhibit spurious numerical oscillation (if the time increment is too short). The guideline in Ref. [Hibbitt, Karlsson and Sorensen (2004)] suggests that the time increment (Δt) should be slightly greater than $\Delta l^2 / (6 \cdot \theta \cdot D)$, where D is the diffusivity and Δl is a typical element dimension.

2.2 3-D hybrid moisture element formulation

In the formulation, the material properties are assumed to be linearly elastic and isotropic, but are heterogeneous from each sub-domain. The separate formulations for the two sub-domains are derived (index notation is used) as follows:

(I) Formulation in the inter-phase sub-domain:

The similar partition concept [Guo (1979)] is applied to the inter-phase sub-domain, as shown in Fig. 2(a). The meshing steps are described as follows: First, the outer boundary (element domain boundary), Γ_0, is properly discretized with the total number of $2m$ master nodes (represented by symbol "o"), ordered in a counter-clockwise direction. Second, when the global origin O located in the inclusion region is chosen as a similar partition center, and when a certain number of chosen element-layers s and a certain compatible proportionality constant $c \in (0,1)$ are taken, similar polygons $\Gamma_1, \Gamma_2, \cdots, \Gamma_s$ of Γ_0 are constructed with center O according to the proportionality constants $c^1, c^2, \cdots, c^s$, respectively. The region bounded between Γ_{i-1} and Γ_i is called the *i-th* element-layer (i= 1, 2, $\cdots$, s). Third, straight lines are drawn from the origin to the master nodes, and each individual Γ_i is regularly discretized, similar to Γ_0. The nodal number and coordinates of the nodes on each individual Γ_i can be determined from the master node coordinates under geometrically similar conditions. Fourth, each element-layer is auto-meshed into several four-node quadrilateral elements that are similar to one another from the element-layers in a radial direction.

Both the element moisture capacitance matrix $[M_e]$ and the element moisture conductance matrix $[K_e]$ for each quadrilateral element in the element layer of the inter-phase sub-domain (i.e. the region between boundaries Γ_0 and Γ_1) can be calculated and assembled into global matrices, i.e. $[M]$ and $[K]$, using the conventional finite element formulation. The assembled matrices of the outermost element-layer (1st element-layer) are therefore expressed as

$$[M] = \begin{bmatrix} M_a & -B^T \\ -B & M_b \end{bmatrix}_{2\mathrm{m}\times 2\mathrm{m}} \tag{11}$$

and

$$[K] = \begin{bmatrix} K_a & -A^T \\ -A & K_b \end{bmatrix}_{2\mathrm{m}\times 2\mathrm{m}}, \tag{12}$$

where M_a, M_b, and B are sub-matrices of the assembled matrix $[M]$ with identical dimensions $m \times m$, K_a, K_b, and A are sub-matrices of the assembled matrix $[K]$ with identical dimensions $m \times m$, and B^T and A^T are the transposes of B and A,

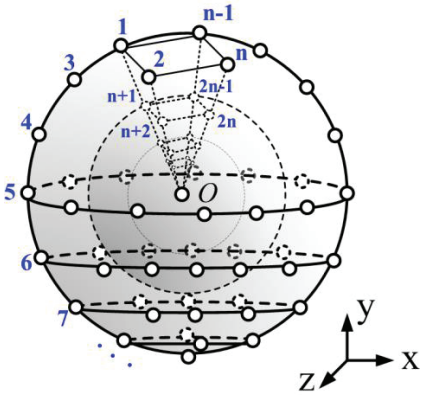

Heterogeneous hybrid moisture element

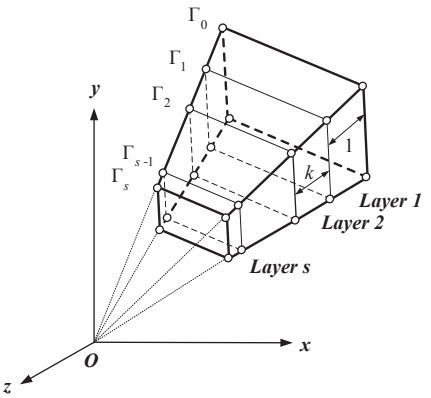

(a) inter-phase sub-domain

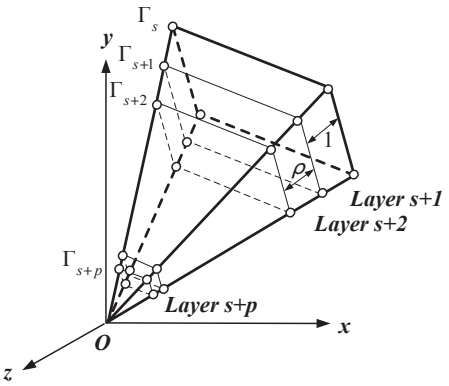

(b) inclusion sub-domain

Figure 2: Heterogeneous hybrid moisture element mesh: (a) inter-phase sub-domain; and (b) inclusion sub-domain

respectively. Since the element layer matrices $[M]$ and $[K]$ are globally symmetrical and banded, matrices M_a, M_b, K_a, and K_b are also symmetrical and banded.

The nodal moisture wetness vector W_i^n of the nodes on Γ_i at the time t_n is defined as

$$W_i^n \equiv \left[\begin{array}{cccc} W_1^{i,n} & W_2^{i,n} & \cdots & W_m^{i,n} \end{array} \right]^T. \tag{13}$$

The nodal loading vector P_i of the nodes on Γ_i is defined as

$$P_i \equiv \left[\begin{array}{cccc} P_1^i & P_2^i & \cdots & P_m^i \end{array} \right]^T. \tag{14}$$

According to the similarity principle, it is obvious that the element moisture capacitance matrices of all of the element-layers are in dimensional dependence on the ratio k^3 and the element moisture conductance matrices of all of the element-layers are identical. Hence, in accordance with Eq. (10), we can express the element matrices of the *s* element-layers (from the *1st* element-layer to the *s-th* element-layer) as *s* sets of algebraic equations, namely,

for layer 1

$$\begin{aligned}&\left\{\begin{bmatrix} M_a & -B^T \\ -B & M_b \end{bmatrix} + \theta\cdot\Delta t\cdot\begin{bmatrix} K_a & -A^T \\ -A & K_b \end{bmatrix}\right\}\cdot\begin{bmatrix} W_0^{n+1} \\ W_1^{n+1} \end{bmatrix} = \\ &\left\{\begin{bmatrix} M_a & -B^T \\ -B & M_b \end{bmatrix} + \phi\cdot\Delta t\cdot\begin{bmatrix} K_a & -A^T \\ -A & K_b \end{bmatrix}\right\}\cdot\begin{bmatrix} W_0^{n} \\ W_1^{n} \end{bmatrix} + \Delta t\cdot\begin{bmatrix} P_0 \\ P_1 \end{bmatrix}\end{aligned} \tag{15}$$

for layer 2

$$\begin{aligned}&\left\{k^3\cdot\begin{bmatrix} M_a & -B^T \\ -B & M_b \end{bmatrix} + \theta\cdot\Delta t\cdot k\begin{bmatrix} K_a & -A^T \\ -A & K_b \end{bmatrix}\right\}\cdot\begin{bmatrix} W_1^{n+1} \\ W_2^{n+1} \end{bmatrix} = \\ &\left\{k^3\cdot\begin{bmatrix} M_a & -B^T \\ -B & M_b \end{bmatrix} + \phi\cdot\Delta t\cdot k\begin{bmatrix} K_a & -A^T \\ -A & K_b \end{bmatrix}\right\}\cdot\begin{bmatrix} W_1^{n} \\ W_2^{n} \end{bmatrix} + \Delta t\cdot\begin{bmatrix} -P_1 \\ P_2 \end{bmatrix}\end{aligned} \tag{16}$$

for layer 3

$$\begin{aligned}&\left\{k^6\cdot\begin{bmatrix} M_a & -B^T \\ -B & M_b \end{bmatrix} + \theta\cdot\Delta t\cdot k^2\begin{bmatrix} K_a & -A^T \\ -A & K_b \end{bmatrix}\right\}\cdot\begin{bmatrix} W_2^{n+1} \\ W_3^{n+1} \end{bmatrix} = \\ &\left\{k^6\cdot\begin{bmatrix} M_a & -B^T \\ -B & M_b \end{bmatrix} + \phi\cdot\Delta t\cdot k^2\begin{bmatrix} K_a & -A^T \\ -A & K_b \end{bmatrix}\right\}\cdot\begin{bmatrix} W_2^{n} \\ W_3^{n} \end{bmatrix} + \Delta t\cdot\begin{bmatrix} -P_2 \\ P_3 \end{bmatrix}\end{aligned} \tag{17}$$

$\vdots$

for layer *s*

$$\begin{aligned}&\left\{k^{3(s-1)}\cdot\begin{bmatrix} M_a & -B^T \\ -B & M_b \end{bmatrix} + \theta\cdot\Delta t\cdot k^{(s-1)}\begin{bmatrix} K_a & -A^T \\ -A & K_b \end{bmatrix}\right\}\cdot\begin{bmatrix} W_{s-1}^{n+1} \\ W_s^{n+1} \end{bmatrix} = \\ &\left\{k^{3(s-1)}\cdot\begin{bmatrix} M_a & -B^T \\ -B & M_b \end{bmatrix} + \phi\cdot\Delta t\cdot k^{(s-1)}\begin{bmatrix} K_a & -A^T \\ -A & K_b \end{bmatrix}\right\}\cdot\begin{bmatrix} W_{s-1}^{n} \\ W_s^{n} \end{bmatrix} \\ &+\Delta t\cdot\begin{bmatrix} -P_{s-1} \\ P_s \end{bmatrix}\end{aligned} \tag{18}$$

Extracting each algebraic equation, combining the second equation for the *i-th* element-layer, and the first equation for the *(i+1)-th* element-layer, and letting

$X = M_b + k^3 \cdot M_a$ and $Y = K_b + k \cdot K_a$, we have

$$\begin{aligned}&(M_a + \theta \cdot \Delta t \cdot K_a) \cdot W_0^{n+1} + \left(-B^T - \theta \cdot \Delta t \cdot A^T\right) \cdot W_1^{n+1} \\ &= (M_a + \phi \cdot \Delta t \cdot K_a) \cdot W_0^n + \left(-B^T - \phi \cdot \Delta t \cdot A^T\right) \cdot W_1^n + \Delta t \cdot P_0\end{aligned} \tag{19}$$

$$\begin{aligned}&(-B - \theta \cdot \Delta t \cdot A) \cdot W_0^{n+1} + (X + \theta \cdot \Delta t \cdot Y) \cdot W_1^{n+1} + \left(-c^2 B^T - \theta \cdot \Delta t \cdot A^T\right) \cdot W_2^{n+1} \\ &= (-B - \phi \cdot \Delta t \cdot A) \cdot W_0^n + (X + \phi \cdot \Delta t \cdot Y) \cdot W_1^n + \left(-c^2 B^T - \phi \cdot \Delta t \cdot A^T\right) \cdot W_2^n \\ &\vdots\end{aligned} \tag{20}$$

$$\begin{aligned}&\left(-k^{3(i-1)} B - \theta \cdot \Delta t \cdot k^{(i-1)} \cdot A\right) \cdot W_{i-1}^{n+1} + \left(k^{3(i-1)} X + \theta \cdot \Delta t \cdot k^{(i-1)} \cdot Y\right) \cdot W_i^{n+1} \\ &+ \left(-k^{3i} B^T - \theta \cdot \Delta t \cdot k^i \cdot A^T\right) \cdot W_{i+1}^{n+1} \\ &= \left(-k^{3(i-1)} B - \phi \cdot \Delta t \cdot k^{(i-1)} \cdot A\right) \cdot W_{i-1}^n + \left(k^{3(i-1)} X + \phi \cdot \Delta t \cdot k^{(i-1)} \cdot Y\right) \cdot W_i^n \\ &+ \left(-k^{3i} B^T - \phi \cdot \Delta t \cdot k^i \cdot A^T\right) \cdot W_{i+1}^n \\ &\vdots\end{aligned} \tag{21}$$

$$\begin{aligned}&\left(-k^{3(s-2)} B - \theta \cdot \Delta t \cdot k^{(s-2)} \cdot A\right) \cdot W_{s-2}^{n+1} + \left(k^{3(s-2)} X + \theta \cdot \Delta t \cdot k^{(s-2)} \cdot Y\right) \cdot W_{s-1}^{n+1} \\ &+ \left(-k^{3(s-1)} B^T - \theta \cdot \Delta t \cdot k^{(s-1)} \cdot A^T\right) \cdot W_s^{n+1} \\ &= \left(-k^{3(s-2)} B - \phi \cdot \Delta t \cdot k^{(s-2)} \cdot A\right) \cdot W_{s-2}^n + \left(k^{3(s-2)} X + \phi \cdot \Delta t \cdot k^{(s-2)} \cdot Y\right) \cdot W_{s-1}^n \\ &+ \left(-k^{3(s-1)} B^T - \phi \cdot \Delta t \cdot k^{(s-1)} \cdot A^T\right) \cdot W_s^n\end{aligned} \tag{22}$$

$$\begin{aligned}&\left(-k^{3(s-1)} B - \theta \cdot \Delta t \cdot k^{(s-1)} \cdot A\right) \cdot W_{s-1}^{n+1} + \left(k^{3(s-1)} M_b + \theta \cdot \Delta t \cdot k^{(s-1)} \cdot K_b\right) \cdot W_s^{n+1} \\ &= \left(-k^{3(s-1)} B - \phi \cdot \Delta t \cdot k^{(s-1)} \cdot A\right) \cdot W_{s-1}^n \\ &+ \left(k^{3(s-1)} M_b + \phi \cdot \Delta t \cdot k^{(s-1)} \cdot K_b\right) \cdot W_s^n + \Delta t \cdot P_s\end{aligned} \tag{23}$$

(II) Formulation in the inclusion sub-domain:

The partition processes for the inclusion sub-domain, as shown in Fig. 2(b), are similar to the processes for the inter-phase sub-domain. The inner boundary Γ_s of the inter-phase region is exactly the outer boundary of the inclusion region. Also, when the global origin O is chosen as the similar partition center and when another proportionality constant c and element-layers p are taken, similar polygons Γ_{s+1}, Γ_{s+2}, $\cdots$, Γ_{s+p} of Γ_s are generated with center O, according to the relative proportionality constants c^1, c^2, $\cdots$, c^p. The region bounded between Γ_{j-1} and Γ_j is called the *j-th* element-layer ($j = s$+1, s+2, $\cdots$, $s+p$). The assembled matrices of the p element-layers (from the s+1-*th* element-layer to the s+p-*th* element-layer) can be expressed as p sets of algebraic equations, namely,

for layer s+1

$$\begin{aligned}
&\left\{\begin{bmatrix} M_{\Delta a} & -B_{\Delta}^T \\ -B_{\Delta} & M_{\Delta b} \end{bmatrix} + \theta\cdot\Delta t\cdot\begin{bmatrix} K_{\Delta a} & -A_{\Delta}^T \\ -A_{\Delta} & K_{\Delta b} \end{bmatrix}\right\}\cdot\begin{bmatrix} W_s^{n+1} \\ W_{s+1}^{n+1} \end{bmatrix} = \\
&\left\{\begin{bmatrix} M_{\Delta a} & -B_{\Delta}^T \\ -B_{\Delta} & M_{\Delta b} \end{bmatrix} + \phi\cdot\Delta t\cdot\begin{bmatrix} K_{\Delta a} & -A_{\Delta}^T \\ -A_{\Delta} & K_{\Delta b} \end{bmatrix}\right\}\cdot\begin{bmatrix} W_s^{n} \\ W_{s+1}^{n} \end{bmatrix} + \Delta t\cdot\begin{bmatrix} P_s \\ P_{s+1} \end{bmatrix}
\end{aligned} \tag{24}$$

for layer s+2

$$\begin{aligned}
&\left\{c^3\cdot\begin{bmatrix} M_{\Delta a} & -B_{\Delta}^T \\ -B_{\Delta} & M_{\Delta b} \end{bmatrix} + \theta\cdot\Delta t\cdot c\begin{bmatrix} K_{\Delta a} & -A_{\Delta}^T \\ -A_{\Delta} & K_{\Delta b} \end{bmatrix}\right\}\cdot\begin{bmatrix} W_{s+1}^{n+1} \\ W_{s+2}^{n+1} \end{bmatrix} = \\
&\left\{c^3\cdot\begin{bmatrix} M_{\Delta a} & -B_{\Delta}^T \\ -B_{\Delta} & M_{\Delta b} \end{bmatrix} + \phi\cdot\Delta t\cdot c\begin{bmatrix} K_{\Delta a} & -A_{\Delta}^T \\ -A_{\Delta} & K_{\Delta b} \end{bmatrix}\right\}\cdot\begin{bmatrix} W_{s+1}^{n} \\ W_{s+2}^{n} \end{bmatrix} + \Delta t\cdot\begin{bmatrix} -P_{s+1} \\ P_{s+2} \end{bmatrix}
\end{aligned} \tag{25}$$

for layer s+3

$$\begin{aligned}
&\left\{c^6\cdot\begin{bmatrix} M_{\Delta a} & -B_{\Delta}^T \\ -B_{\Delta} & M_{\Delta b} \end{bmatrix} + \theta\cdot\Delta t\cdot c^2\begin{bmatrix} K_{\Delta a} & -A_{\Delta}^T \\ -A_{\Delta} & K_{\Delta b} \end{bmatrix}\right\}\cdot\begin{bmatrix} W_{s+2}^{n+1} \\ W_{s+3}^{n+1} \end{bmatrix} = \\
&\left\{c^6\cdot\begin{bmatrix} M_{\Delta a} & -B_{\Delta}^T \\ -B_{\Delta} & M_{\Delta b} \end{bmatrix} + \phi\cdot\Delta t\cdot c^2\begin{bmatrix} K_{\Delta a} & -A_{\Delta}^T \\ -A_{\Delta} & K_{\Delta b} \end{bmatrix}\right\}\cdot\begin{bmatrix} W_{s+2}^{n} \\ W_{s+3}^{n} \end{bmatrix} + \Delta t\cdot\begin{bmatrix} -P_{s+2} \\ P_{s+3} \end{bmatrix} \\
&\vdots
\end{aligned} \tag{26}$$

for layer *s*+p

$$\begin{aligned}
&\left\{c^{3(p-1)}\cdot\begin{bmatrix} M_{\Delta a} & -B_{\Delta}^{T} \\ -B_{\Delta} & M_{\Delta b}\end{bmatrix}+\theta\cdot\Delta t\cdot c^{(p-1)}\begin{bmatrix} K_{\Delta a} & -A_{\Delta}^{T} \\ -A_{\Delta} & K_{\Delta b}\end{bmatrix}\right\}\cdot\begin{bmatrix} W_{s+p-1}^{n+1} \\ W_{s+p}^{n+1}\end{bmatrix}= \\
&\left\{c^{3(p-1)}\cdot\begin{bmatrix} M_{\Delta a} & -B_{\Delta}^{T} \\ -B_{\Delta} & M_{\Delta b}\end{bmatrix}+\phi\cdot\Delta t\cdot c^{(p-1)}\begin{bmatrix} K_{\Delta a} & -A_{\Delta}^{T} \\ -A_{\Delta} & K_{\Delta b}\end{bmatrix}\right\}\cdot\begin{bmatrix} W_{s+p-1}^{n} \\ W_{s+p}^{n}\end{bmatrix} \\
&+\Delta t\cdot\begin{bmatrix} -P_{s+p-1} \\ P_{s+p}\end{bmatrix}
\end{aligned} \tag{27}$$

Extracting each algebraic equation, combining the second equation for the *j-th* element-layer and the first equation for the *(j+1)-th* element-layer, and letting $R=M_{\Delta b}+c^{3}M_{\Delta a}$ and $Q=K_{\Delta b}+c\cdot K_{\Delta a}$, we have

$$\begin{aligned}
&(M_{\Delta a}+\theta\cdot\Delta t\cdot K_{\Delta a})\cdot W_{s}^{n+1}+\left(-B_{\Delta}^{T}-\theta\cdot\Delta t\cdot A_{\Delta}^{T}\right)\cdot W_{s+1}^{n+1} \\
&=(M_{\Delta a}+\phi\cdot\Delta t\cdot K_{\Delta a})\cdot W_{s}^{n}+\left(-B_{\Delta}^{T}-\phi\cdot\Delta t\cdot A_{\Delta}^{T}\right)\cdot W_{s+1}^{n}-\Delta t\cdot P_{s}
\end{aligned} \tag{28}$$

$$\begin{aligned}
&(-B_{\Delta}-\theta\cdot\Delta t\cdot A_{\Delta})\cdot W_{s}^{n+1}+(R+\theta\cdot\Delta t\cdot Q)\cdot W_{s+1}^{n+1}+\left(-c^{3}\cdot B_{\Delta}^{T}-\theta\cdot\Delta t\cdot c\cdot A_{\Delta}^{T}\right)\cdot W_{s+2}^{n+1} \\
&=(-B_{\Delta}-\phi\cdot\Delta t\cdot A_{\Delta})\cdot W_{s}^{n}+(R+\phi\cdot\Delta t\cdot Q)\cdot W_{s+1}^{n}+\left(-c^{3}\cdot B_{\Delta}^{T}-\phi\cdot\Delta t\cdot c\cdot A_{\Delta}^{T}\right)\cdot W_{s+2}^{n} \\
&\vdots
\end{aligned} \tag{29}$$

$$\begin{aligned}
&\left(-c^{3(j-(s+1))}B_{\Delta}-\theta\cdot\Delta t\cdot c^{(j-(s+1))}\cdot A_{\Delta}\right)\cdot W_{j-1}^{n+1} \\
&+\left(c^{3(j-(s+1))}R+\theta\cdot\Delta t\cdot c^{(j-(s+1))}\cdot Q\right)\cdot W_{j}^{n+1}+\left(-c^{3(j-s)}B_{\Delta}^{T}-\theta\cdot\Delta t\cdot c^{(j-s)}\cdot A_{\Delta}^{T}\right)\cdot W_{j+1}^{n+1} \\
&=\left(-c^{3(j-(s+1))}B_{\Delta}-\phi\cdot\Delta t\cdot c^{(j-(s+1))}\cdot A_{\Delta}\right)\cdot W_{j-1}^{n} \\
&+\left(c^{3(j-(s+1))}R+\phi\cdot\Delta t\cdot c^{(j-(s+1))}\cdot Q\right)\cdot W_{j}^{n}+\left(-c^{3(j-s)}B_{\Delta}^{T}-\phi\cdot\Delta t\cdot c^{(j-s)}\cdot A_{\Delta}^{T}\right)\cdot W_{j+1}^{n} \\
&\vdots
\end{aligned} \tag{30}$$

$$\begin{aligned}
&\left(-c^{3(p-2)}B_{\Delta}-\theta\cdot\Delta t\cdot c^{(p-2)}\cdot A_{\Delta}\right)\cdot W_{s+p-2}^{n+1}+\left(c^{3(p-2)}R+\theta\cdot\Delta t\cdot c^{(p-2)}\cdot Q\right)\cdot W_{s+p-1}^{n+1} \\
&+\left(-c^{3(p-1)}B_{\Delta}^{T}-\theta\cdot\Delta t\cdot c^{(p-1)}\cdot A_{\Delta}^{T}\right)\cdot W_{s+p}^{n+1} \\
&=\left(-c^{3(p-2)}B_{\Delta}-\phi\cdot\Delta t\cdot c^{(p-2)}\cdot A_{\Delta}\right)\cdot W_{s+p-2}^{n}+\left(c^{3(p-2)}R+\phi\cdot\Delta t\cdot c^{(p-2)}\cdot Q\right)\cdot W_{s+p-1}^{n} \\
&+\left(-c^{3(p-1)}B_{\Delta}^{T}-\phi\cdot\Delta t\cdot c^{(p-1)}\cdot A_{\Delta}^{T}\right)\cdot W_{s+p}^{n}
\end{aligned}$$

(31)

$$\begin{aligned}
&\left(-c^{3(p-1)}B_\Delta - \theta\cdot\Delta t\cdot c^{(p-1)}\cdot A_\Delta\right)\cdot W_{s+p-1}^{n+1} + \left(c^{3(p-1)}M_{\Delta b} + \theta\cdot\Delta t\cdot c^{(p-1)}\cdot K_{\Delta b}\right)\cdot W_{s+p}^{n+1}\\
&= \left(-c^{3(p-1)}B_\Delta - \phi\cdot\Delta t\cdot c^{(p-1)}\cdot A_\Delta\right)\cdot W_{s+p-1}^{n}\\
&+ \left(c^{3(p-1)}M_{\Delta b} + \phi\cdot\Delta t\cdot c^{(p-1)}\cdot K_{\Delta b}\right)\cdot W_{s+p}^{n} + \Delta t\cdot P_{s+p}
\end{aligned} \tag{32}$$

Let $N_{s+p} = c^{3(p-1)}M_{\Delta b} + \phi\cdot\Delta t\cdot c^{(p-1)}K_{\Delta b}$, $V_{s+p} = c^{3(p-1)}M_{\Delta b} + \theta\cdot\Delta t\cdot c^{(p-1)}K_{\Delta b}$ and $FF_{s+p} = \Delta t\cdot P_{s+p}$. Substituting them into Eq. (32), we have

$$W_{s+p}^{n+1} = V_{s+p}^{-1}\cdot\begin{bmatrix} -\left(-c^{3(p-1)}B_\Delta - \theta\cdot\Delta t\cdot c^{(p-1)}\cdot A_\Delta\right)\cdot W_{s+p-1}^{n+1} \\ +\left(-c^{3(p-1)}B_\Delta - \phi\cdot\Delta t\cdot c^{(p-1)}\cdot A_\Delta\right)\cdot W_{s+p-1}^{n} \\ +N_{s+p}\cdot W_{s+p}^{n} + FF_{s+p}\end{bmatrix} \tag{33}$$

By substituting Eq. (33) into Eq. (31), we get

$$\begin{aligned}
&(-c^{3(p-2)}B_\Delta - \theta\cdot\Delta t\cdot c^{(p-2)}A_\Delta)\cdot W_{s+p-2}^{n+1} + [(c^{3(p-2)}R + \theta\cdot\Delta t\cdot c^{(p-2)}Q)\\
&+ (-c^{3(p-1)}B_\Delta^T - \theta\cdot\Delta t\cdot c^{(p-1)}A_\Delta^T)\cdot V_{s+p}^{-1}\cdot(c^{3(p-1)}B_\Delta + \theta\cdot\Delta t\cdot c^{(p-1)}A_\Delta)]\cdot W_{s+p-1}^{n+1}\\
&= (-c^{3(p-2)}B_\Delta - \phi\cdot\Delta t\cdot c^{(p-2)}A_\Delta)\cdot W_{s+p-2}^{n}\\
&+ [(c^{3(p-2)}R + \phi\cdot\Delta t\cdot c^{(p-2)}Q) -\\
&(-c^{3(p-1)}B_\Delta^T - \theta\cdot\Delta t\cdot c^{(p-1)}A_\Delta^T)\cdot V_{s+p}^{-1}\cdot(-c^{3(p-1)}B_\Delta - \phi\cdot\Delta t\cdot c^{(p-1)}A_\Delta)]\cdot W_{s+p-1}^{n}\\
&+ [(-c^{3(p-1)}B_\Delta^T - \phi\cdot\Delta t\cdot c^{(p-1)}A_\Delta^T)\\
&- (-c^{3(p-1)}B_\Delta^T - \theta\cdot\Delta t\cdot c^{(p-1)}A_\Delta^T)\cdot V_{s+p}^{-1}\cdot N_{s+p}]\cdot W_{s+p}^{n}\\
&- (-c^{3(p-1)}B_\Delta^T - \theta\cdot\Delta t\cdot c^{(p-1)}A_\Delta^T)\cdot V_{s+p}^{-1}\cdot FF_{s+p}
\end{aligned} \tag{34}$$

When Eq. (34) is compared with Eq. (32), three iteration formulas can be inferred:

$$\begin{aligned}
N_i = &\left(c^{3(i-(s+1))}R + \phi\cdot\Delta t\cdot c^{(i-(s+1))}\cdot Q\right) +\\
&\left(-c^{3(i-s)}B_\Delta^T - \theta\cdot\Delta t\cdot c^{(i-s)}A_\Delta^T\right)\cdot V_{i+1}^{-1}\cdot\left(c^{3(i-s)}B_\Delta + \phi\cdot\Delta t\cdot c^{(i-s)}A_\Delta\right)
\end{aligned} \tag{35}$$

$$\begin{aligned}
V_i = &\left(c^{3(i-(s+1))}R + \theta\cdot\Delta t\cdot c^{(i-(s+1))}\cdot Q\right)\\
&+\left(-c^{3(i-s)}B_\Delta^T - \theta\cdot\Delta t\cdot c^{(i-s)}\cdot A_\Delta^T\right)\cdot V_{i+1}^{-1}\cdot\left(c^{3(i-s)}B_\Delta + \theta\cdot\Delta t\cdot c^{(i-s)}A_\Delta\right)
\end{aligned} \tag{36}$$

$$\begin{aligned} FF &= [(-c^{3(i-s)}B_\Delta^T - \phi\cdot\Delta t\cdot c^{(i-s)}A_\Delta^T) \\ &- (-c^{3(i-s)}B_\Delta^T - \theta\cdot\Delta t\cdot c^{(i-s)}A_\Delta^T)\cdot V_{i+1}^{-1}\cdot N_{i+1}]\cdot W_{i+1}^n \\ &- (-c^{3(i-s)}B_\Delta^T - \theta\cdot\Delta t\cdot c^{(i-s)}A_\Delta^T)\cdot V_{i+1}^{-1}\cdot FF_{i+1} \end{aligned} \tag{37}$$

where $i = s$+1, s+2, s+3,$\cdots$, $s+p$-1.

By substituting the above three iteration formulas into Eq. (34), we get

$$\begin{aligned} &\left(-c^{3(p-2)}B_\Delta - \theta\cdot\Delta t\cdot c^{(p-2)}A_\Delta\right)\cdot W_{s+p-2}^{n+1} + V_{s+p-1}\cdot \mathbf{W_{s+p-1}^{n+1}} \\ &= \left(-c^{3(p-2)}B_\Delta - \phi\cdot\Delta t\cdot c^{(p-2)}A_\Delta\right)\cdot W_{s+p-2}^{n} + N_{s+p-1}\cdot W_{s+p-1}^{n} + FF_{s+p-1} \end{aligned} \tag{38}$$

Rearranging Eq. (38) and another iteration formula can be inferred as

$$\begin{aligned} W_j^{n+1} &= -V_j^{-1}\cdot\left(-c^{3(j-(s+1))}B_\Delta - \theta\cdot\Delta t\cdot c^{(j-(s+1))}A_\Delta\right)\cdot W_{j-1}^{n+1} \\ &+ V_j^{-1}\cdot\begin{bmatrix} \left(-c^{3(j-(s+1))}B_\Delta - \phi\cdot\Delta t\cdot c^{(j-(s+1))}A_\Delta\right)\cdot W_{j-1}^{n} \\ +N_j\cdot W_j^n + FF_j \end{bmatrix} \end{aligned} \tag{39}$$

where $j = s$+1, s+2, s+3,$\cdots$, $s+p$.

From Eq. (39), we have

$$\begin{aligned} W_{s+1}^{n+1} &= -V_{s+1}^{-1}\cdot(-B_\Delta - \theta\cdot\Delta t\cdot A_\Delta)\cdot W_s^{n+1} \\ &+ V_{s+1}^{-1}\cdot\left[(-B_\Delta - \phi\cdot\Delta t\cdot A_\Delta)\cdot W_s^n + N_{s+1}\cdot W_{s+1}^n + FF_{s+1}\right] \end{aligned} \tag{40}$$

By substituting Eq. (40) into Eq. (28), we get

$$\begin{aligned} &(M_{\Delta a} + \theta\cdot\Delta t\cdot K_{\Delta a})\cdot W_s^{n+1} \\ &+ \left(-B_\Delta^T - \theta\cdot\Delta t\cdot A_\Delta^T\right)\cdot\left\{\begin{matrix} -V_{s+1}^{-1}\cdot(-B_\Delta - \theta\cdot\Delta t\cdot A_\Delta)\cdot W_s^{n+1} \\ +V_{s+1}^{-1}\cdot\left[(-B_\Delta - \phi\cdot\Delta t\cdot A_\Delta)\cdot W_s^n + N_{s+1}\cdot W_{s+1}^n + FF_{s+1}\right] \end{matrix}\right\} \\ &= (M_{\Delta a} + \phi\cdot\Delta t\cdot K_{\Delta a})\cdot W_s^n + \left(-B_\Delta^T - \phi\cdot\Delta t\cdot A_\Delta^T\right)\cdot W_{s+1}^n - \Delta t\cdot P_s \end{aligned} \tag{41}$$

Rearranging Eq. (41), we have

$$\begin{aligned} &\left[(M_{\Delta a} + \theta\cdot\Delta t\cdot K_{\Delta a}) - \left(-B_\Delta^T - \theta\cdot\Delta t\cdot A_\Delta^T\right)\cdot V_{s+1}^{-1}\cdot(-B_\Delta - \theta\cdot\Delta t\cdot A_\Delta)\right]\cdot W_s^{n+1} \\ &= (M_{\Delta a} + \phi\cdot\Delta t\cdot K_{\Delta a})\cdot W_s^n + \left(-B_\Delta^T - \phi\cdot\Delta t\cdot A_\Delta^T\right)\cdot W_{s+1}^n - \Delta t\cdot P_s \\ &- \left(-B_\Delta^T - \theta\cdot\Delta t\cdot A_\Delta^T\right)\cdot V_{s+1}^{-1}\cdot\left[(-B_\Delta - \phi\cdot\Delta t\cdot A_\Delta)\cdot W_s^n + N_{s+1}\cdot W_{s+1}^n + FF_{s+1}\right] \end{aligned}$$

(42)

Equation (42) can be expressed in the concise form

$$H_{(\text{inclusion})} \cdot W_s^{n+1} = F_{(\text{inclusion})} \tag{43}$$

where $H_{(\text{inclusion})}$ and $F_{(\text{inclusion})}$ denote the equivalent hybrid moisture capacitance/conductance matrix and associated loading vector for the inclusion sub-domain, respectively. Along the inclusion/inter-phase interface Γ_s, however, the moisture wetness compatibility and force equilibrium must be satisfied. Therefore, equations (23) and (43) are combined and we have

$$\begin{aligned}
&(-k^{3(s-1)}B - \theta \cdot \Delta t \cdot k^{(s-1)} \cdot A) \cdot W_{s-1}^{n+1} \\
&+ \{H_{(inclusion)} + (k^{3(s-1)}M_b + \theta \cdot \Delta t \cdot k^{(s-1)} \cdot K_b)\} \cdot W_s^{n+1} \\
&= (-k^{3(s-1)}B - \phi \cdot \Delta t \cdot k^{(s-1)} \cdot A) \cdot W_{s-1}^{n} \\
&+ [-(-B_\Delta^T - \theta \cdot \Delta t \cdot A_\Delta^T) \cdot V_{s+1}^{-1} \cdot (B_\Delta - \phi \cdot \Delta t \cdot A_\Delta) \\
&+ k^{3(s-1)}M_b + M_{\Delta a} + \phi \cdot \Delta t \cdot (K_{\Delta a} + k^{(s-1)} \cdot K_b)] \cdot W_s^n \\
&+ [-(-B_\Delta^T - \theta \cdot \Delta t \cdot A_\Delta^T) \cdot V_{s+1}^{-1} \cdot N_{s+1} + (-B_\Delta^T - \phi \cdot \Delta t \cdot A_\Delta^T)] \cdot W_{s+1}^n \\
&- (-B_\Delta^T - \theta \cdot \Delta t \cdot A_\Delta^T) \cdot V_{s+1}^{-1} \cdot FF_{s+1}
\end{aligned} \tag{44}$$

Again, let

$$\begin{aligned}
N_s = &- \left(-B_\Delta^T - \theta \cdot \Delta t \cdot A_\Delta^T\right) \cdot V_{s+1}^{-1} \cdot (-B_\Delta - \phi \cdot \Delta t \cdot A_\Delta) \\
&+ k^{3(s-1)}M_b + M_{\Delta a} + \phi \cdot \Delta t \cdot \left(K_{\Delta a} + k^{(s-1)} \cdot K_b\right),
\end{aligned}$$

$$V_s = H_{(inclusion)} + \left(k^{3(s-1)}M_b + \theta \cdot \Delta t \cdot k^{(s-1)} \cdot K_b\right)$$

and

$$\begin{aligned}
FF_s = &\left[\left(-B_\Delta^T - \phi \cdot \Delta t \cdot A_\Delta^T\right) - \left(-B_\Delta^T - \theta \cdot \Delta t \cdot A_\Delta^T\right) \cdot V_{s+1}^{-1} \cdot N_{s+1}\right] \cdot W_{s+1}^n \\
&- \left(-B_\Delta^T - \theta \cdot \Delta t \cdot A_\Delta^T\right) \cdot V_{s+1}^{-1} \cdot FF_{s+1}.
\end{aligned}$$

Four parameters representing the inter-phase sub-domain can be inferred:

$$\begin{aligned}
N_i = &k^{3(i-1)}X + \phi \cdot \Delta t \cdot k^{(i-1)} \cdot Y \\
&- \left(-k^{3(i)}B^T - \theta \cdot \Delta t \cdot k^{(i)} \cdot A^T\right) \cdot V_{i+1}^{-1} \cdot \left(-k^{3(i)}B - \phi \cdot \Delta t \cdot k^{(i)} \cdot A\right)
\end{aligned} \tag{45}$$

$$\begin{aligned} V_i =& k^{3(i-1)}X + \theta \cdot \Delta t \cdot k^{(i-1)} \cdot Y \\ & - \left(-k^{3(i)}B^T - \theta \cdot \Delta t \cdot k^{(i)} \cdot A^T\right) \cdot V_{i+1}^{-1} \cdot \left(-k^{3(i)}B - \theta \cdot \Delta t \cdot k^{(i)} \cdot A\right) \end{aligned} \tag{46}$$

$$\begin{aligned} FF_i =& \left(-k^{3(i)}B^T - \phi \cdot \Delta t \cdot k^{(i)} \cdot A^T - \left(-k^{3(i)}B^T - \theta \cdot \Delta t \cdot k^{(i)} \cdot A^T\right) \cdot V_{i+1}^{-1} \cdot N_{i+1}\right) \cdot W_{i+1}^n \\ & - \left(-k^{3(i)}B^T - \theta \cdot \Delta t \cdot k^{(i)} \cdot A^T\right) \cdot V_{i+1}^{-1} \cdot FF_{i+1} \end{aligned} \tag{47}$$

$$\begin{aligned} W_j^{n+1} =& -V_j^{-1} \cdot \left(-k^{3(i-1)}B - \theta \cdot \Delta t \cdot k^{(i-1)} \cdot A\right) \cdot W_{j-1}^{n+1} \\ & + V_j^{-1} \cdot \left[\left(-k^{3(i-1)}B - \phi \cdot \Delta t \cdot k^{(i-1)} \cdot A\right) \cdot W_{j-1}^n + N_j \cdot W_j^n + FF_j\right] \end{aligned} \tag{48}$$

where i= 1, 2, 3,$\cdots$, s-1; and j= 1, 2, 3,$\cdots$, s.

Since N_s, V_s and FF_s are known, then N_{s-1}, N_{s-2}, $\cdots$, N_1;V_{s-1}, V_{s-2}, $\cdots$, V_1; FF_{s-1}, FF_{s-2}, $\cdots$, FF_1 can be iterated out using equations (45), (46) and (47), respectively. From Eq. (48), we have the unknown moisture wetness $W_1^{n+1} = -V_1^{-1} \cdot (-B - \theta \cdot \Delta t \cdot A) \cdot W_0^{n+1} + V_1^{-1} \cdot [(-B - \phi \cdot \Delta t \cdot A) \cdot W_0^n + N_1 \cdot W_1^n + FF_1]$ at the new time-level t_{n+1}. By substituting W_1^{n+1} into Eq. (19), we obtain the most important equation, that is,

$$\begin{aligned} & \left[(M_a + \theta \cdot \Delta t \cdot K_a) - \left(-B^T - \theta \cdot \Delta t \cdot A^T\right) \cdot V_1^{-1} \cdot (-B - \theta \cdot \Delta t \cdot A)\right] \cdot W_0^{n+1} \\ & = \left[(M_a + \phi \cdot \Delta t \cdot K_a) \cdot W_0^n + \left(-B^T - \phi \cdot \Delta t \cdot A^T\right) \cdot W_1^n + \Delta t \cdot P_0\right] \\ & - \left(-B^T - \theta \cdot \Delta t \cdot A^T\right) \cdot V_1^{-1} \cdot [(-B - \phi \cdot \Delta t \cdot A) \cdot W_0^n + N_1 \cdot W_1^n + FF_1] \end{aligned} \tag{49}$$

Equation (49) can be expressed in the concise form

$$H_Z \cdot W_0^{n+1} = F_Z \tag{50}$$

where H_Z and F_Z denote the equivalent hybrid moisture capacitance/conductance matrix and associated loading vector for the heterogeneous hybrid moisture element, respectively. The H_Z term preserves the symmetry characteristic of the global hybrid moisture capacitance/conductance matrix in FE representation. The F_Z term contains both effects of the outer surface traction and the known moisture wetness at the current time t_n. Once F_Z is determined, W_0^{n+1} can be obtained from Eq. (49). Then W_1^{n+1}, W_2^{n+1}, $\cdots$, W_s^{n+1}, $\cdots$, and W_{s+p}^{n+1} can be obtained sequentially from equations (48) and (39).

In the current analysis, it is assumed that the boundary flux is zero and that only the Dirichlet boundary condition is applied, i.e. concentrations only are prescribed at

the boundaries. Therefore, the element matrix equation can be rewritten as:

$$\begin{aligned}
&\left[(M_a+\theta\cdot\Delta t\cdot K_a)-\left(-B^T-\theta\cdot\Delta t\cdot A^T\right)\cdot V_1^{-1}\cdot(-B-\theta\cdot\Delta t\cdot A)\right]\cdot W_0^{n+1}\\
&=\left[(M_a+\phi\cdot\Delta t\cdot K_a)\cdot W_0^n+\left(-B^T-\phi\cdot\Delta t\cdot A^T\right)\cdot W_1^n\right]\\
&-\left(-B^T-\theta\cdot\Delta t\cdot A^T\right)\cdot V_1^{-1}\cdot\left[(-B-\phi\cdot\Delta t\cdot A)\cdot W_0^n+N_1\cdot W_1^n+FF_1\right]
\end{aligned}\tag{51}$$

where $P_i=0$ (i = 1, 2,$\cdots$, s, s+1,$\cdots$, $s+p$).

2.3 Implementation of coupled HHME-FE scheme

The HHMEM is derived from the conventional FEM in space discretization as well as the θ-method in time discretization. Then it uses the similarity characteristic of element mass/stiffness and the matrix condensing procedures to solve transient moisture diffusion problems in heterogeneous materials and structures. A series of layer-wise elements with similar shapes are virtually generated within the problem domain. The numerous resultant degrees of freedom (DOFs) are condensed and transformed to those on the boundary master nodes only by means of derived recurrence formulas.

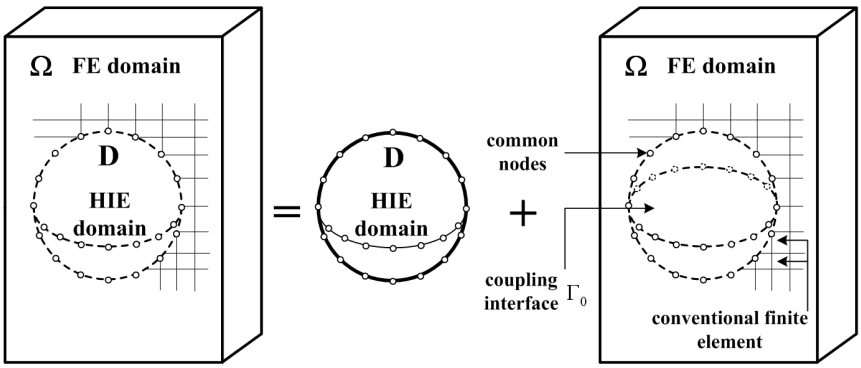

Figure 3: Schematic diagram of the coupled HHME-FE scheme

When the problem domain includes multiple sub-domains with repetitive geometry (e.g., particle inclusions), it is not favorable to employ finite elements to model an entire domain with a large number of elements. Therefore, we propose a coupled HHME-FE scheme that uses only HHMEs to subdivide the entire domain into several sub-domains without the use of finite elements. To illustrate the assembling scheme shown in Fig. 3, the global model is partitioned into two separate domains which are separated from the coupling interface Γ_0, namely Ω and D, modeled

using the HHME and FE, respectively. The master nodes on the outer boundary of the HHMEs are taken from interface common nodes between the HHME and FE sub-domains. Because each HHME equivalent hybrid moisture capacitance/conductance matrix, H_Z, is pre-determined (see Section 2.2), the elements can be treated as regular finite elements, and their HHME H_Z matrices are assembled into the global combined capacitance/conductance matrix.

The related HHMEM numerical procedures and the coupled HHME-FE scheme were programmed and executed using self-written codes in MATLAB language [Kwon and Bang (2000)]. In the proposed approach, the total number of DOFs is remarkably reduced, and hence the modeling and computational effort are substantially decreased.

3 Validation of 3D HHME-FE model

This section presents two examples to validate the performance of the proposed HHME-FE modeling approach. Fig. 4 (right panel) shows the HHME-FE computational model exhibiting three inclusions, in which the length, width, and thickness dimensions are $70\mu m$, $40\mu m$, and $30\mu m$, respectively. In this figure, D represents the HHME sub-domain and Ω represents the FE sub-domain. The HHME domain is separated into two regions containing the inclusion region (i.e. the particles) and the inter-phase region. The material properties of the inter-phase region are identical to those in the FE sub-domain (i.e. the resin matrix). Therefore, the inter-phase is not explicitly modeled and it is assumed that a perfect bond exists between the particles and the resin matrix. As shown, the inclusions are circular and possess a radius 11.5 times smaller than the model length. A moisture condition of 35 $^{\circ}C$/85% RH is applied at the left edge and thus the moisture permeates from the exposed surface on the left of the model and diffuses to the right. The moisture-related material properties of the resin matrix and the permeable particles in the applied moisture conditions of 35$^{\circ}C$/85% RH are presented in Tab. 2 [Laurenzi, Albrizio and Marchetti (2008)].

Table 2: Material properties

Property	particles	Resin matrix
Moisture diffusivity (35$^{\circ}C$/85% RH)	3.630×10^{-8} mm^2/s	5.183×10^{-7} mm^2/s
Saturated moisture concentration (35$^{\circ}C$/85% RH)	2.375×10^{-6} g/mm^3	9.386×10^{-6} g/mm^3

The right panels of Fig. 4-6 show the coupled HHME-FE modeling results for the moisture profiles at three different times. The HHMEM parameters of the inclusion and inter-phase regions are $c = 0.6$ and $k = 0.922$, and $p = 7$ and $s = 5$, respectively. In the HHME-FE model, 294 master nodes were used. In addition, 98 nodes were used in each of the three HHME sub-domains and 19,669 four-node tetrahedron elements were used in the FE sub-domain. The corresponding results obtained from the conventional FEM scheme are presented in the left panels for comparison purposes. In the conventional FE model, the number of elements totaled 22,949 and the total number of nodes was 4,625. Tab. 3 provides the comparisons of both methods based on the number of degrees of freedom (DOFs). A comparison of the two sets of transient moisture distributions reveals that the HHME-FE results are in satisfactory agreement with the FEM results.

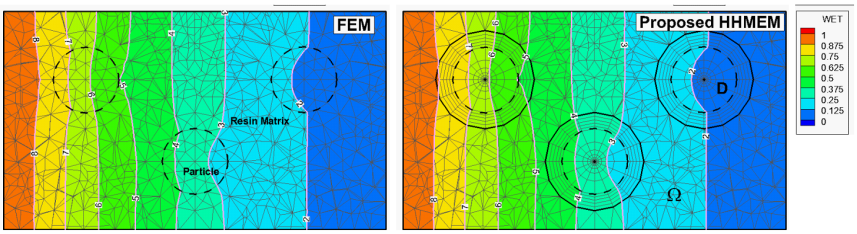

Figure 4: Moisture distribution at the 1200s for moisture conditions of 35°*C*/85%RH

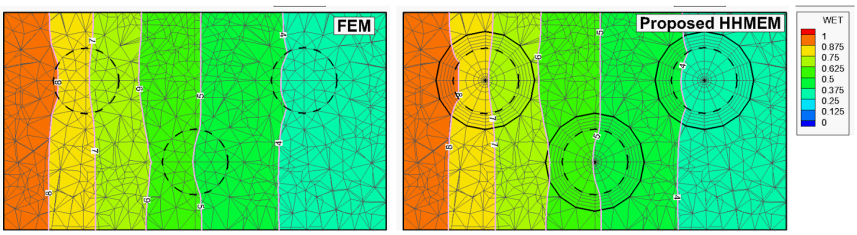

Figure 5: Moisture distribution at the 2400s for moisture conditions of 35°*C*/85%RH

In the second validation example, Fig. 7 plots the variation for the level of wetness in the resin matrix after various time steps in an HHME-FE computational model in which the length, width, and thickness dimensions were $163\mu m$, $43\mu m$, and $23\mu m$, respectively, and the volume fraction of particles was 5%. The HHMEM parameters of the inclusion and inter-phase regions are $c = 0.6$ and $k = 0.907$, and $p = 9$

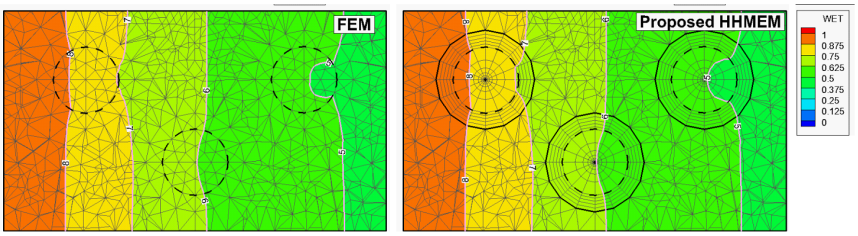

Figure 6: Moisture distribution at the 3600s for moisture conditions of 35°C/85%RH

Table 3: DOFs of the HHME-FE and FEM approaches

Numerical method	Total nodes	Total DOFs	Equivalent DOFs
HHME-FE	4138	4138	7666
FEM	4625	4625	4625

and $s = 6$, respectively. In the HHME-FE model, a total of 1,568 master nodes were used. In addition, 98 nodes were used in each of the 16 HHME sub-domains and 31,670 four-node tetrahedron elements were used in the FE sub-domain. In the conventional FE model, the number of elements totaled 49,729 and the total number of nodes was 9,810. Tab. 4 provides the comparisons between both methods based on the number of DOFs. It can be seen that the results obtained from the HHME-FE method are in satisfactory agreement with those obtained from the FEM approach and that the HHME-FE method contains far fewer DOFs than does the full FEM.

As described, the proposed HHMEM provides a straightforward and efficient means of modeling transient moisture diffusion in a resin matrix filled with multiple particles. This is because only one HHME equivalent hybrid moisture capacitance/conductance matrix needs to be calculated for all HHMEs that possess the same properties. Furthermore, all DOFs related to the HHME domain are condensed and transformed to form a combined element with only the master node DOFs. Therefore, the coupled HHME-FE method considerably reduces the execution time in the mesh modeling stage, the total number of DOFs, and the PC memory storage requirements.

Table 4: DOFs of the HME-FE and FEM approaches

Numerical method	Total nodes	Total DOFs	Equivalent DOFs
HHME-FE	7,177	7,177	30,697
FEM	9,810	9,810	9,810

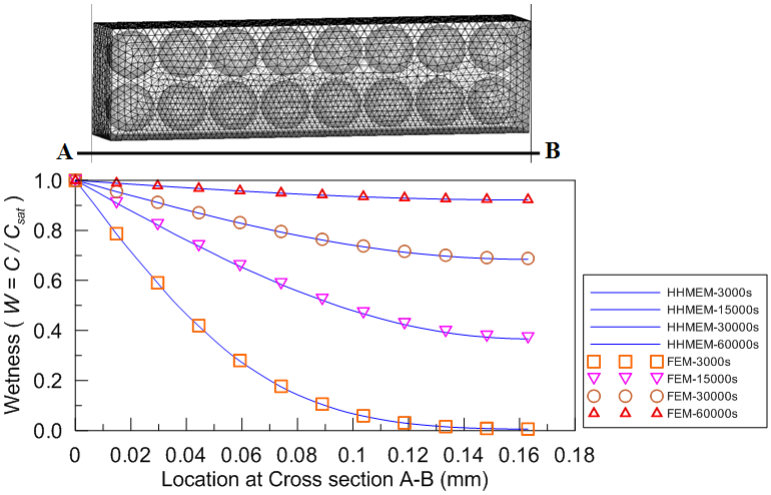

Figure 7: Moisture diffusion from 200^{th} to 5000^{th} time step

4 Numerical example

Regarding the particle-reinforced composite analyzed in this study, the particles were assumed to be distributed regularly in the resin matrix. An examination of the moisture diffusion properties of a heterogeneous composite reveals multiple permeable particles of various volume fractions, i.e. 5 to 30% processed in five equal steps. The resin matrix was assumed to be heterogeneous and to possess a length, width, and thickness of $163\mu m$, $43\mu m$, and $23\mu m$, respectively. A moisture condition of 35 $^{\circ}C$/85% RH was applied at the left side of the structure. The moisture-related material properties of the resin matrix and the permeable particles in the applied moisture conditions of 35$^{\circ}C$/85% RH are presented in Table 2 [Laurenzi, Albrizio and Marchetti (2008)].

4.1 Influence of volume fraction of particles on moisture diffusion

The coupled HHME-FE scheme was applied to investigate the moisture diffusion characteristics of the resin matrix that contained regular distributed particles of var-

ious volume fractions, i.e. 5 to 30% processed in five equal steps. In the HHME sub-domain of the HHME-FE computational model, the material properties of the inter-phase region were identical to those in the matrix region (i.e. the resin matrix). Therefore, the inter-phase is not modeled explicitly. Furthermore, it was assumed that a perfect bonding existed between the particles and the resin matrix. Thus, various particle volume fractions could be modeled without modifying the original model simply by controlling the size of the inter-phase region within the HHME domain. The HHMEM parameters of the respective inclusion and inter-phase regions for each volume fraction studied are listed in Table 5. In the particle HHME-FE model, a total of 1,568 master nodes were used. In addition, 98 nodes were used in each of the 16 HHME sub-domains, and 31,670 four-node tetrahedron elements were used in the FE sub-domain.

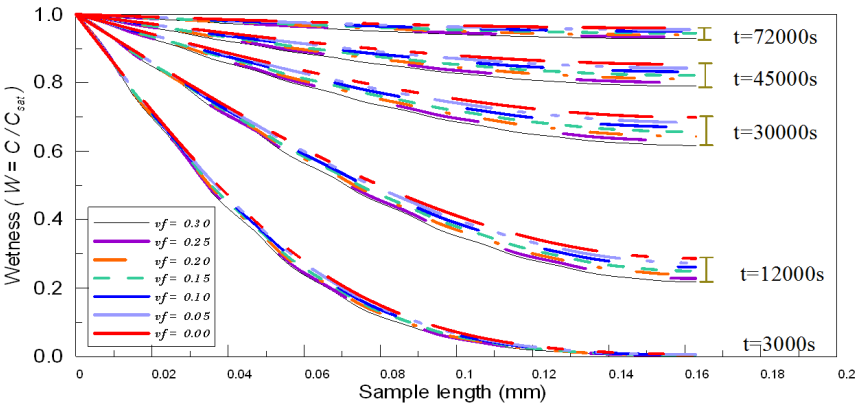

Figure 8: Effects of varying volume fractions of particles in resin matrix of moisture diffusion

Table 5: HHMEM parameters for each studied volume fraction

Volume fraction	Inclusion		Inter-phase	
	λ	p	c	s
5%	0.6	9	0.907	6
10%	0.6	9	0.931	5
15%	0.6	9	0.946	4
20%	0.6	9	0.957	3
25%	0.6	9	0.972	2
30%	0.6	9	0	0

Fig. 8 shows the effect of varying the volume fractions of particles, i.e. 5 to 30% processed in five steps, in the resin matrix that is adjacent to the lower boundary of the moisture diffusion. The moisture that reaches the far end of the resin matrix reduces as the volume fraction of the particles increases. The physical explanation for this is that the regularly distributed particles impede moisture transfer, particularly at higher volume fractions. The result implies that a particle-reinforced composite can be constructed that uses a resin matrix containing a high volume fraction of particles to provide long-term durability with maximum protection against the effects of moisture penetration. Most importantly, various particle volume fractions can be modeled without modifying the original model simply by controlling the size of the inter-phase region within the HHME domain. This advantage of the HHME approach becomes particularly apparent when the scheme is applied to investigate the relationship between the particle volume fraction and the moisture diffusion characteristics of a heterogeneous composite material filled with multiple particles.

4.2 A convenient method to inverse calculating the effective diffusion coefficient

The effective diffusion coefficient, D_{eff}, is an important material property used to calculate moisture diffusion problems. To inverse calculate the D_{eff},

first, the 3D HHMEM was employed to simulate moisture diffusing process with various particle volume fraction; the data of wetness v. s. time were recorded and plotted in Fig. 9. A wetness that rose to 0.95 meant that the particle-reinforced composite material reached a 95% saturated concentration. On the other hand, the particle-reinforced composite almost can't fully impede the moisture penetration. The time to reach a wetness of 0.95 at the far end of the resin matrix was labeled $t_{0.95}$.

After $t_{0.95}$ was obtained, a reference finite element model with the same size of the previous particle-reinforced composite was built, but the material properties of the permeable particles are replaced by the resin matrix and the same boundary conditions and time steps are applied. This reference numerical model can be implemented by changing the diffusion coefficient of the resin matrix and obtaining the corresponding trial $t_{0.95}$ from the simulation results. The numerical iteration process continues until the trial $t_{0.95}$ equal to the $t_{0.95}$ based on the 3D-HHMEM results. The calculated diffusion coefficient of the resin matrix was selected as the D_{eff}. The corresponding results are presented in Table 6.

As can be seen in Table 6, the $t_{0.95}$ of the volume fraction of the particle-reinforced composite were varied from 0 to 30% processed in six equal steps. The results reveal that the moisture penetration time was retard by 13,620 seconds because of a 30% volume fraction of the particle-reinforced composite, which represents a

20.23% effect on the hindrance of moisture penetration. It is also easy to see that the effective diffusion coefficient was enhanced by $0.871*10^{-7}$ square millimeter per second; that means it can reduce the effective diffusion coefficient by 16.8%.

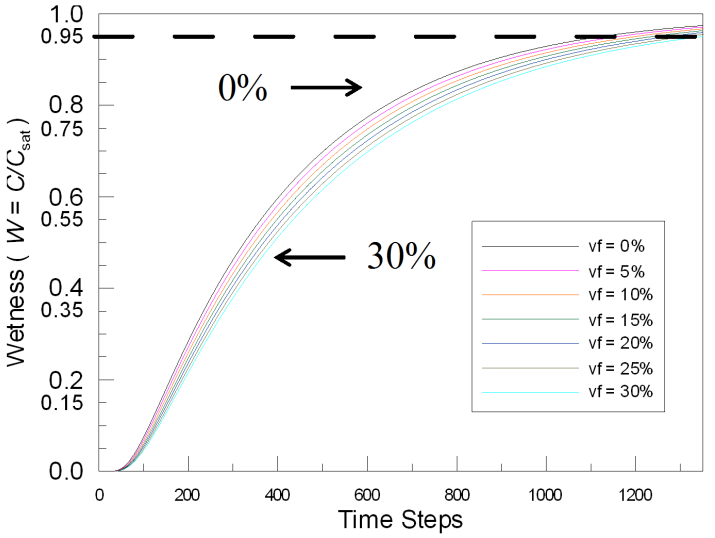

Figure 9: Moisture diffusion process with Effects of varying volume fractions of particles in resin matrix

Table 6: The effective diffusion coefficient by inverse calculating for each studied volume fraction

Volume fraction	*0%*	*5%*	*10%*	*15%*	*20%*	*25%*	*30%*
$t_{0.95}(s)$	67320	69600	71880	74160	76380	78660	80940
D_{eff} $(mm^2/s)^*$ 10^{-7}	5.183	5.016	4.857	4.709	4.570	4.438	4.312

5 Conclusion

A 3D-HHMEM designed to solve moisture diffusion problems was developed in this study. In this method, the heterogeneous region was subdivided into two

sub-domains containing the inclusion and the inter-phase portions. The characteristics of HHME were determined by an equivalent hybrid moisture capacitance/conductance matrix. This matrix was calculated by using the conventional FEM in space discretization and the θ-method in time discretization that exhibits similar mass/stiffness properties and matrix condensing operations. A coupled HHME-FE scheme was developed and implemented using the MATLAB language.

The performance of the proposed HHME-FE method was validated by comparing the results obtained for the moisture distribution profiles in a heterogeneous resin composite with those obtained from the conventional FEM scheme. Secondly, the analysis examined the effect of the volume fraction of particles on the rate of moisture diffusion. The results revealed that the amount of moisture penetrating the resin composite reduced considerably as the volume fraction of the particles increased. Therefore, it can be inferred that a particle-reinforced composite can be constructed using a resin matrix with a high volume fraction of particles to protect the inner components against moisture ingression. Finally, the effective diffusion coefficient containing a varying volume fraction of particles was investigated based on the analysis and revealed that a 30% volume fraction of the particle-reinforced composite retarded the time of moisture penetration by 20.23% and reduced the effective diffusion coefficient by 16.8%.

Several key advantages of the 3D-HHMEM can be listed as follows.

1. In the computational model, the regions of the resin occupied by the particles are all replaced by HHMEs such that only one HHME-equivalent hybrid moisture capacitance/conductance matrix requires calculation for all HHMEs that possess the same characteristics. Thus, the total number of DOFs in the computational model and the PC memory storage and processing requirements are considerably reduced.

2. Various volume fractions of particles can be modeled without modifying the original model simply by controlling the size of the inter-phase region within the HHME domain.

3. The results obtained from the proposed method are in satisfactory agreement with those of the conventional FEM scheme.

4. Through the use of a fast iteration numerical method, the effective diffusion coefficient introduced in this study is extremely convenient and easy to calculate. Its use in this large and complex numerical analysis (i.e. particle-reinforced composite) is speedy and efficient.

Acknowledgment

The current authors gratefully acknowledge the financial support provided to this study by the Hanbell Precise Machinery CO., under Grant NO. 101-B48, and National Science Council, Taiwan, ROC., under Grant NO. NSC101-2923-E-194-002-MY3.

References

Browning, C. E.; Husman, G. E.; Whitney, J. M. (1977): Moisture effects in epoxy resin matrix composites. *Composite Materials: Testing and Design, ASTM STP,* vol. 617, pp. 481-496.

Crank, J.; Park, G. S. (1956): *The Mathematics of Diffusion*. Oxford University Press.

Crank, J.; Nicolson, P. (1947): A practical method for numerical evaluation of solutions of partial differential equations of the heat conduction type. *Proceedings of the Cambridge Philosophical Society*, vol. 43, pp. 50–64.

Dong, L.; Atluri, S. N. (2012a): T-Trefftz Voronoi cell finite elements with elastic/rigid inclusions or voids for micromechanical analysis of composite and porous materials. *CMES: Computer Modeling in Engineering & Sciences*, vol. 83, no.2, pp. 183-219.

Dong, L.; Atluri, S. N. (2012b): Development of 3D T-Trefftz Voronoi Cell Finite Elements with/without Spherical Voids &/or Elastic/Rigid Inclusions for Micromechanical Modeling of Heterogeneous Materials. *CMC: Computers Materials and Continua*, vol. 29, no. 2, pp. 169.

Dong, L.; Atluri, S. N. (2012c): Development of 3 D Trefftz Voronoi Cells with Ellipsoidal Voids &/or Elastic/Rigid Inclusions for Micromechanical Modeling of Heterogeneous Materials. *CMC: Computers Materials and Continua*, vol. 30, no.1, pp. 39.

Guo, Z. H. (1979): Similar isoparametric elements. *Sci. Bull.*, vol. 24, no. 13, pp. 577-582.

Hibbitt, D.; Karlsson, B.; Sorensen, P. (2004): *ABAQUS User's Manual Version 6.5*. Pawtucket, RI.

Kawaguchi, T.; Pearson, R. A. (2003): The effect of particle-matrix adhesion on the mechanical behavior of glass filled epoxies: Part 1. A study on yield behavior and cohesive strength. *Polymer*, vol. 44, pp. 4229-4238.

Kwon, Y.W.; Bang, H. (2000): *The Finite Element Method using MATLAB, second ed.* CRC Press, New York.

Laurenzi, S.; Albrizio, T.; Marchetti, M. (2008): Modeling of Moisture Diffusion in Carbon Braided Composites. *International Journal of Aerospace Engineering*, vol. 2008, article id. 294681, 10 pages.

Lewis, R. W.; Morgan, K.; Thomas, H. R.; Seetharamu, K. N. (1996): *The Finite Element Method in Heat Transfer Analysis*, Wiley, New York, pp. 81-87.

Liu, D. S.; Chiou, D. Y. (2003a): A coupled IEM/FEM approach for solving the elastic problems with multiple cracks. *Int. J. Solids Struct.*, vol. 40, pp. 1973-1993.

Liu, D. S.; Chiou, D. Y. (2003b): 3D IEM formulation with an IEM/FEM coupling scheme for solving elastostatic problems. *Adv. Eng. Softw.*, vol. 34, pp. 309-320.

Liu, D. S.; Chiou, D. Y. (2005): 2D infinite element modeling for elastostatic problems with geometric singularity and unbounded domain. *Comput. Struct.*, vol. 83, pp. 2086-2099

Liu, D. S.; Chiou, D. Y.; Lin C. H. (2004): A hybrid 3D thermo-elastic infinite element modeling for area-arrey package solder joints. *Finite Elem. Anal. Des.*, vol. 40, pp. 1703-1727.

Liu, D. S.; Chiou, D. Y. (2004): Modeling of inclusion with interphases in heterogeneous material using the infinite element method. *Comp. Mater. Sci.*, vol. 31, pp. 405-420.

Liu, D. S.; Chen, C. Y.; Chiou, D. Y. (2005): 3D Modeling of a composite material reinforced with multiple thickly coated particles using the infinite element method. *CMES: Computer Modeling in Engineering & Sciences*, vol. 9, pp. 179-191.

Liu, D. S.; Zhuang, Z. W.; Chung, C. L. (2009): Modeling of Moisture Diffusion in Heterogeneous Epoxy Resin Containing Multiple Randomly Distributed Particles Using Hybrid Moisture Element Method. *CMC: Computers Materials & Continua*, vol. 13, pp. 89-113.

Liu, D. S., Zhuang, Z. W., Lyu, S. R., Chung, C. L.; Lin, P. C. (2011): Modeling of Moisture Diffusion in Permeable Fiber-Reinforced Polymer Composites Using Heterogeneous Hybrid Moisture Element Method. *CMC: Computers Materials & Continua,* vol. 26, pp. 111-136.

Pahr, D. H.; Böhm, H. J. (2008): Assessment of mixed uniform boundary conditions for predicting the mechanical behavior of elastic and inelastic discontinuously reinforced composites. *CMES: Computer Modeling in Engineering & Sciences*, vol. 34, pp. 117-136.

Shen, C. H.; Springer G. S. (1977): Moisture absorption and desorption of composite materials. *Journal of Composite Materials*, vol. 10, no. 1, pp. 2-20.

Stroeven, M., Askes, H.; Sluys, L.J. (2004): Numerical determination of representative volumes for granular materials. *Computer Methods in Applied Mechanics*

and Engineering, vol. 193, pp. 3221-3238.

Tsai, S. W.; Hahn, H. T. (1980): *Introduction to Composite Materials*. Westport, Conn.: Technomic Pub.

Takashima, S.; Nakagaki, M.; Miyazaki, N. (2007): An elastic-plastic constitutive equation taking account of particle size and its application to a homogenized finite element analysis of a composite material. *CMES: Computer Modeling in Engineering & Sciences*, vol. 20, pp. 193-202.

Vaddadi, P.; Nakamura, T.; Singh, R.P. (2003a): Inverse analysis for transient moisture diffusion through fiber reinforced composites. *Acta Mater.*, vol. 51, no. 1, pp. 177-193.

Vaddadi, P.; Nakamura, T.; Singh, R.P. (2003b): Transient hygrothermal stresses in fiber reinforced composites: A heterogeneous characterization approach. *Compos. Part A*, vol. 34, no. 8, pp. 719-730.

Wong, E. H.; Teo, Y. C.; Lim, T. B. (1998): Moisture diffusion and vapor pressure modeling of IC packaging. *Proceedings of the 48th ECTC*, pp. 1372-1378.

Wong, E. H.; Rajoo, R.; Koh, S. W.; Lim, T. B. (2002): The mechanics and impact of hygroscopic swelling of polymeric materials in electronic packaging. *J. Electron. Packaging*, vol. 124, no, 2, pp. 122-126.

Yang, J.; Yang, Q.; Ma, L.; Liu, W. (2010): Moisture diffusion behavior of permeable fiber-reinforced polymer composite. *Frontiers of Mechanical Engineering in China*, vol. 5, no. 3, pp. 347-352.

Ying, L. A. (1995): *Infinite Element Methods*. Peking University Press and Vieweg Publishing.